



Effect of rare earth doping on magnetic and dielectric properties of NiZnMn ferrites



Xueyun Zhou ^{a,*}, Jun Wang ^b, Dongsheng Yao ^c

^a School of Science, Civil Aviation University of China, Tianjin 300300, China

^b School of Science and Jiangxi Province Key Lab of Microstructure Function Materials, Jiujiang University, Jiujiang, Jiangxi 332005, China

^c Tianjin Key Laboratory of Low Dimensional Materials Physics and Preparing Technology, Faculty of Science, Tianjin University, Tianjin 300072, China

ARTICLE INFO

Article history:

Received 20 August 2022

Received in revised form 16 October 2022

Accepted 26 October 2022

Available online 28 October 2022

Keywords:

Rare earth

Ferrite

Magnetic permeability

Dielectric constant

ABSTRACT

In present work, $\text{RE}_{0.01}\text{Ni}_{0.3}\text{Zn}_{0.4}\text{Mn}_{0.3}\text{Fe}_2\text{O}_4$ ($\text{RE}=\text{Fe, La, Nd, Sm, Gd, Dy, Yb}$) ferrites with strictly controlled main composition were prepared. X-ray diffraction analysis shows that the lattice constant decreases with the increase of atomic number of rare earth. The infrared spectra demonstrate the changes of tetrahedral and octahedral bonds. The saturation magnetization is about 74 emu/g and initial permeability is about 120 for undoped ferrite. They decrease slightly after rare earth doping, but the impact of different rare earth on M_s is same. The Curie temperature of almost all samples is 262 °C. Zero field cooling-field cooling curves demonstrate the existence of spin glass state or superparamagnetism at high temperature. Sm, Gd and Dy doped ferrites have special dielectric properties with more relaxation processes. Appropriate rare earth doping greatly improve the cut-off frequency, dielectric constant for MHz device materials and dielectric loss for GHz electromagnetic wave absorption materials.

© 2022 Elsevier B.V. All rights reserved.

1. Introduction

The molecular formula of single component spinel ferrite is: MeFe_2O_4 , in which Me designates a divalent cation, such as Mn^{2+} , Ni^{2+} , Zn^{2+} , Cu^{2+} , Co^{2+} , etc. The Face-centered cubic (FCC) crystal structure of spinel ferrite is formed by closed packing of oxygen ions. The metal ions fill in two types of interstitial sites known as octahedral (B) site and tetrahedral (A) site. Generally, each metal ion may occupy A or B sites, so the cation distribution can be represented by the formula $(\text{Me}_x^{2+}\text{Fe}_{1-x}^{3+})[\text{Me}_{1-x}^{2+}\text{Fe}_{1+x}^{3+}]_{\text{O}_4}$, where the round and square bracket represent A site and B site respectively and x is a variable.

At present, the complex ferrites composed of two or more kinds of single component ferrite are widely used in microwave absorbers, medical diagnostics, information storage systems, inductor cores, transformer cores and telecommunications etc, because of their excellent magnetic and electric properties, in which MnZn ferrite and NiZn ferrite are typical representatives [1,2]. MnZn ferrite has high initial permeability, low loss and high stability in low frequency applications [3,4]. NiZn ferrite has the advantages of high resistivity, low loss at high frequency and wide frequency band, which make it

useful in high frequency range [5]. So, NiZnMn ferrite is a candidate material with well comprehensive performance and wide frequency range to use. Our previous research shows that pure NiZnMn ferrite can be obtained by vacuum cooling method, and the magnetic properties change regularly in a large range with the increase of Mn replacing Ni [6] in $\text{Ni}_{1-x}\text{Zn}_x\text{Mn}_y\text{Fe}_2\text{O}_4$. Their initial permeability is larger than 100, and Curie temperature is higher than 100 °C, which are suitable for high frequency antenna. In this paper, representative $\text{Ni}_{0.3}\text{Zn}_{0.4}\text{Mn}_{0.3}\text{Fe}_2\text{O}_4$ with moderate initial permeability and Curie temperature was selected as the researched object.

The structure and electromagnetic properties of spinel ferrite can be affected by rare earth doping [7], because of the interaction between 4 f electrons in rare earth and 3d electrons in magnetic cations. Due to the different characteristics of various rare earth ions, their effects are different. Hichem Huili [8] studied the effect of Y and Gd additives on the properties of $\text{Co}_{0.2}\text{Ni}_{0.3}\text{Zn}_{0.5}\text{Fe}_2\text{O}_4$ ferrite and found that the addition of rare earth elements decreases the concentration of $\text{Fe}^{3+}/\text{Fe}^{2+}$ pair, increases the resistivity and the resonance frequency. Curie temperature of the samples increases after Y doping, but decreases after doping Gd. And the loss decreases after Y doping, while increases after doping Gd. Rakesh Kumar Singh [9] studied Pr, Sm and La doped NiZn ferrite and reported that after rare earth doping, the crystal lattice deforms and particle size decreases, resulting in the decrease of magnetic exchange, the saturation magnetization and coercivity. In addition, the dielectric loss

* Corresponding author.

E-mail address: xyz8301@163.com (X. Zhou).

decreases in the range of 100 Hz to 1 MHz. Among all samples, the dielectric constant of Pr doped specimen is the largest, while Sm doped specimen has the smallest dielectric constant. Our research group [10] studied the Gd and La doped NiZnCo ferrite nanoparticles. After rare earth doping, the particle size becomes small, leading to the decrease of saturation magnetization (M_s) and the coercive force (H_c). The doping solubility and the magnitude of drop in magnetic parameter for the two rare earth elements are different. Yanchun Zhang [11] focused on Sm, Ce, La doped $Zn_{0.1}Ba_{0.2}Co_{0.7}Fe_{2-x}Re_xO_4$ ($x = 0.02$) ferrites and reported that doping La^{3+} and Sm^{3+} ions can improve the magnetic properties of ZnBaCo ferrite, but Ce doping cannot. Abdul Majeed [12] observed significant variations of the dielectric properties and direct-current (DC) resistivity with the doping of rare earth metals (La, Nd, Gd, Tb and Dy). Doping rare earth results in enhanced resistivity, due to the increase of gap between ferrous (Fe^{2+}) and ferric (Fe^{3+}) ions, and Tb doped samples has the largest resistivity. Suman Sharma [13] reported that the M_s value of $Ni_{0.5}Co_{0.5}Fe_{1.98}R_{0.02}O_4$ ($R=La, Nd, Sm, Gd, Dy$) ferrites strongly depends on the magnetic moment of rare earth and T_c is dependent on lattice parameter.

According to our observation, there are few studies comparing the effect of different rare earth ions on structural and electromagnetic properties of ferrite, and there is no unified understanding. In view of this, this work aims to explore the impact of rare earth ion on microstructural, low/high-temperature magnetic and dielectric properties of NiZnMn ferrites. In order to eliminate the influence of other factors, the main composition is strictly controlled and a small amount of rare earth is doped to avoid the formation of $REFeO_4$, which is antiferromagnetism.

2. Experiments

The $RE_{0.01}Ni_{0.3}Zn_{0.4}Mn_{0.3}Fe_{1.99}O_4$ ($RE=Fe, La, Nd, Sm, Gd, Dy, Yb$) ferrites were synthesized using the citric acid Sol-Gel method. Actually, the sample with $RE=Fe$ is undoped ferrite. In order to eliminate deviation of major component in the seven samples, the nickel, zinc, manganese and ferric nitrate needed for 0.07 mol $RE_{0.01}Ni_{0.3}Zn_{0.4}Mn_{0.3}Fe_{1.99}O_4$ ferrite were weighed and dissolved in pure water. After well-mixed, the solution was divided into 7 parts on average. Then RE nitrate was added separately. The moles of citric acid are equal to the moles of all cations. The pH value was adjusted to 7 with ammonia. A series of treatment processes including water bath at 80 °C, auto combustion at 220 °C and pre-sintering at 450 °C for 2 h were adopted. Then the PVA was added to the powders. After well ground, the mixture was pressed into an annular specimen with inner diameter of 15 mm and inter diameter of 18 mm, and a disc-shaped pellet with diameter of 20 mm at the pressure of 25 MPa. Finally, they were calcined at 1100 °C for 4 h in a muffle furnace at a heating rate 3 °C /min and cooled in vacuum from 1100 °C to room temperature. During cooling, the atmospheric pressure changes from $1 * 10^5$ Pa to 1000 pa.

The magnetic measurement was performed with physical property measurement system (PPMS DynaCool), and the Zero field cooling-field cooling (ZFC-FC) curves were measured from 10 K to 400 K at 100 Oe. The magnetic permeability was measured with Agilent 4991 A in the frequency range of 1–100 MHz. To measure the electrical properties, pellet was plated with gold electrodes on both sides. Complex permittivity (ϵ) was calculated from equivalent parallel capacitance (C_p) and quality factor (Q) measured using the parallel electrode method by impedance analyzers: Agilent 4991 A in the frequency range of 1 MHz–3 GHz. The other characterization methods used in this paper were referred in previous papers [10,14].

3. Results and discussion

From scanning electron microscope (SEM) patterns in Fig. 1, all samples are porous, and the number of holes increases after rare earth doping. They will have big resistivity for high frequency application. The grains of NiZnMn ferrite show irregular shapes, most particles' size is between 1 μm and 2 μm. After a small amount of rare earth doping, the materials' surface morphology and size distribution hardly change. The average particle size (d) is slightly smaller than that of undoped samples. Because the binding energy of rare earth ions-O²⁻ bond is greater than that of Fe³⁺-O²⁻ bond [15], grain growth is hindered. Light rare earth has little effect, and d is about 1.58 μm for the La, Nd, Sm doped NiZnMn ferrites. However, it is about 1.30 μm for the heavy rare earth doped ferrites. In Fig. 1, obviously there are some bright spots with nanometers, which may be a RE-rich phase[16] or spinel ferrite nanoparticles.

From Fig. 2(a-g), it can be seen that rare earth doping did not change crystal structure. And there are not impurity phases of Fe_2O_3 , Mn_2O_3 or $REFeO_3$ detected by X-ray diffraction (XRD) in all specimens. They show single cubic spinel phase. More details can be obtained by Rietveld refinement with fullprof software. The goodness parameters R_p , R_{wp} , R_{exp} (not corrected for background) are 2.3, 2.88, 2.66, respectively; χ^2 is 1.17; Bragg R factor is 3.338, for the sample without rare earth. The goodness parameters of fitting rare earth doped samples are close to above values. The cell parameters (a_{exp}) are obtained as shown in Fig. 2(i). Yb and Gd doping make the lattice parameters smaller than that of undoped ferrite, which is inconsistent with the fact that the ionic radii of Yb^{3+} (0.868 Å) and Gd^{3+} (0.938 Å) are larger than that of octahedral Fe^{3+} (0.645 Å). Fumie Hiroswa [17] has reported the reduction of lattice parameter in RE-substituted Mg-Zn ferrite, induced by the micro-strain in the internal grain region. The micro-strains were resulted from the compression caused by the difference of the thermal expansion coefficient among the constituent elements or the lattice mismatch between the grain and the grain boundary phase. In contrast, after Sm, Nd and La doping, the lattice parameter increases. It is consistent with the fact that the radii of La^{3+} (1.032 Å), Nd^{3+} (0.983 Å) and Sm^{3+} (0.958 Å) are greater than that of octahedral Fe^{3+} (0.645 Å). Obviously, the influence of ionic radius overwhelms the micro-strain. In addition, with the increase of atomic number of rare earth and the decrease of ionic radii, the lattice constant decreases. This proves the substitution of rare earth metals for Fe.

The molecular formula obtained from refinement is $(Mn_{0.22}Zn_{0.4}Fe_{0.38}) [Mn_{0.08}Ni_{0.3}RE_{0.01}Fe_{1.61}]O_4$. Most Mn ions occupy the tetrahedral (A) sites. Based on the cation distribution, the theoretical lattice parameters (a_{th}) can be calculated using the following equation [18]:

$$a_{th} = \frac{8}{3\sqrt{3}} [r_A + r_O + \sqrt{3}(r_B + r_O)]$$

In which, r_O is the radius of oxygen ions (1.38 Å), r_A and r_B are the average ionic radii of A-site and B-site, determined by the formula:

$$r_A = 0.22r_{Mn^{2+}} + 0.4r_{Zn^{2+}} + 0.38r_{Fe^{3+}}$$

$$r_B = \frac{1}{2}(0.08r_{Mn^{2+}} + 0.3r_{Ni^{2+}} + 0.01r_{RE^{3+}} + 1.61r_{Fe^{3+}})$$

Here $r_{Mn^{2+}}$ is the ionic radius of A-site and B-site taken from Electronic table of Shannon ionic radii according to their coordination [19].

Calculated r_A is 0.5714 Å, r_B is 0.6592, 0.6611, 0.6608, 0.6607, 0.6606, 0.6605 and 0.6603 for the samples with $RE=Fe, La, Nd, Sm, Gd, Dy$ and Yb respectively. Obviously, the change of theoretical lattice parameter (a_{th}) is mainly affected by the octahedral ionic radii (r_B). The theoretical lattice parameters shown in Fig. 2(i) are almost in agreement with the experimental results, indicating that rare

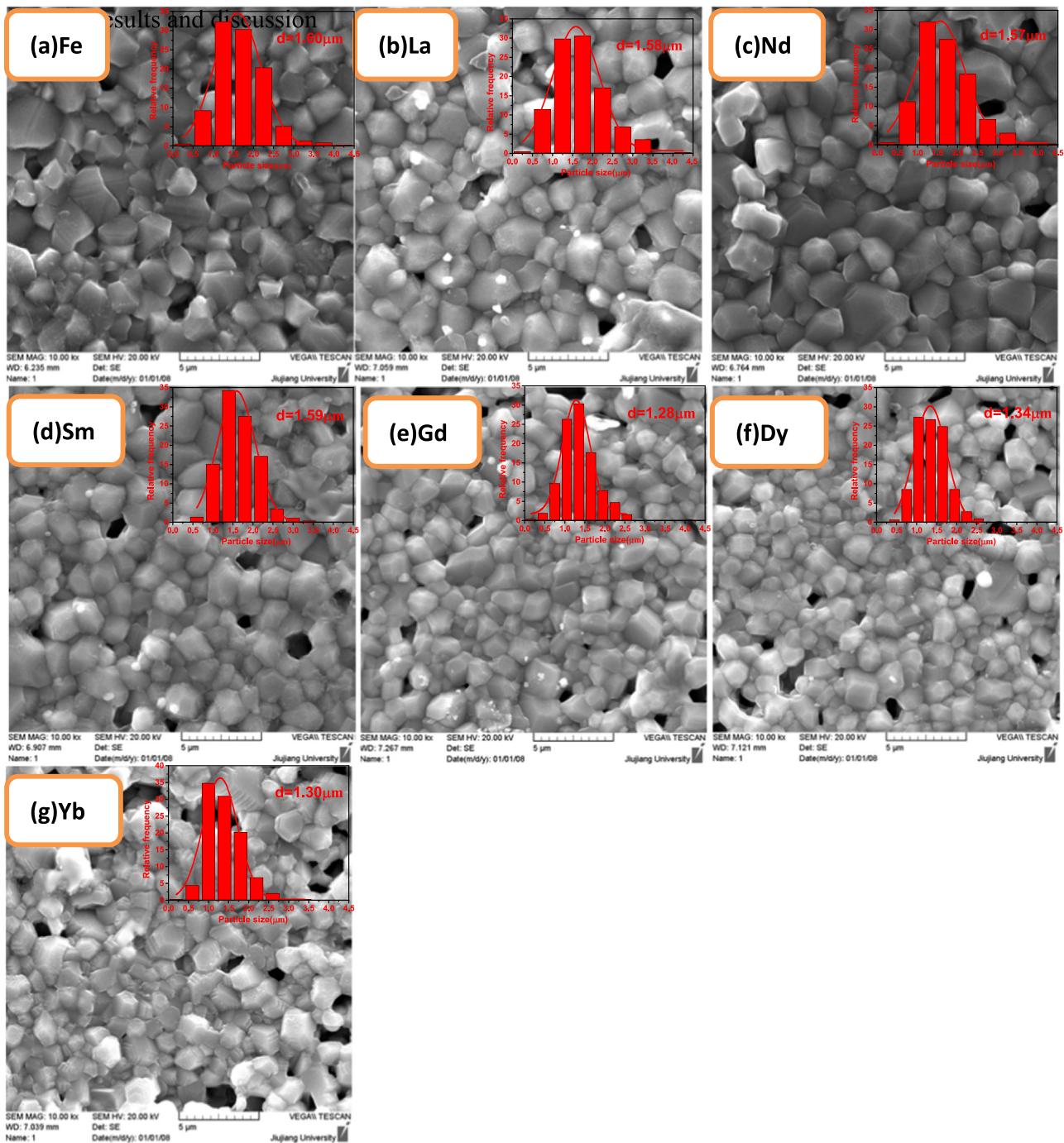


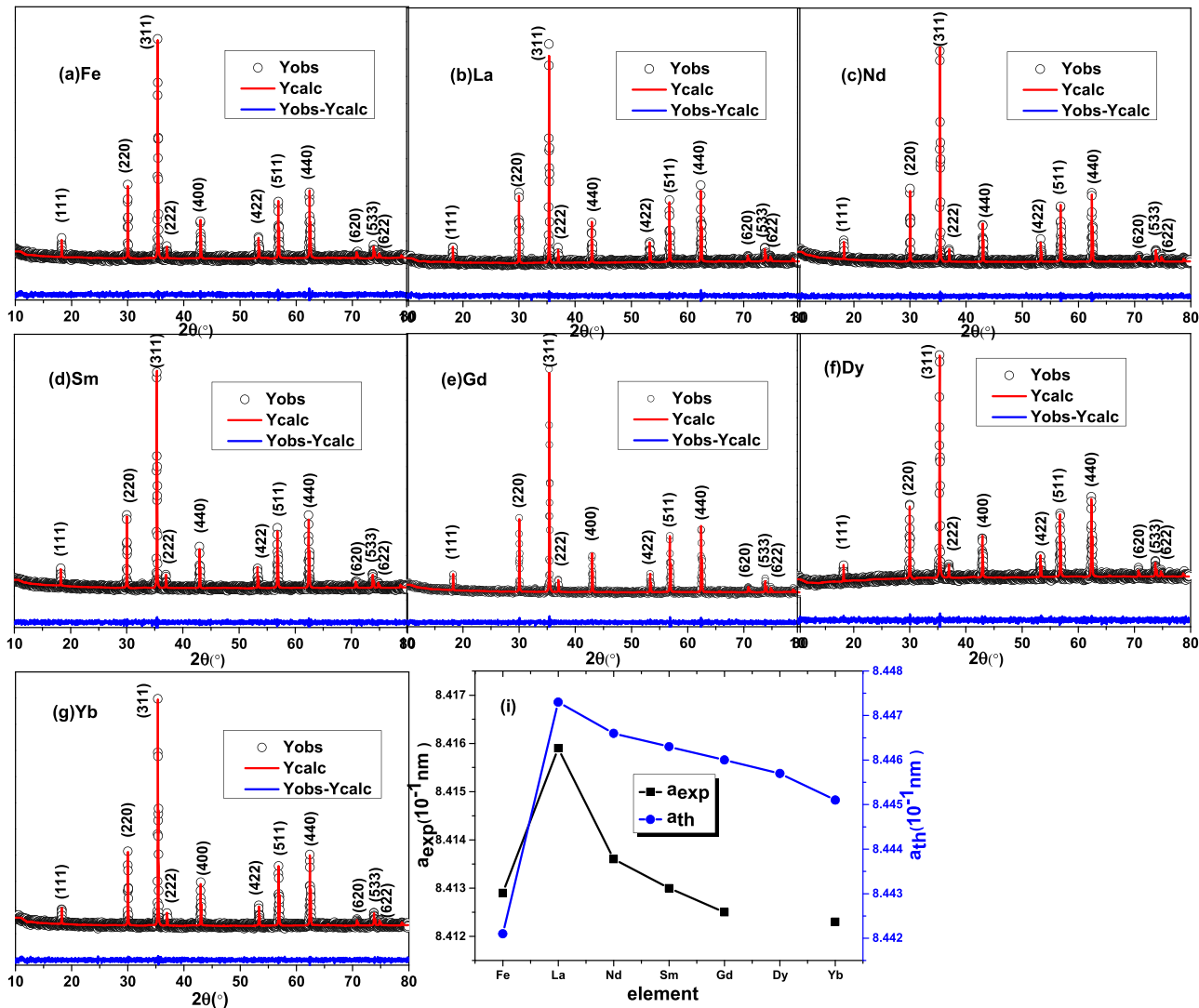
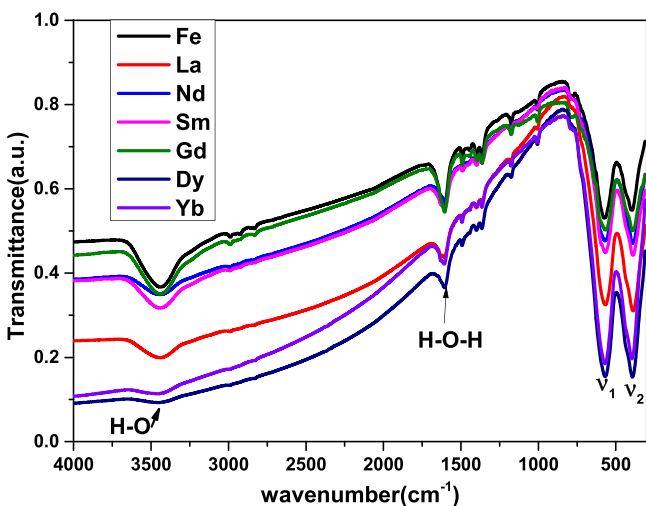
Fig. 1. SEM patterns for annular $\text{RE}_{0.01}\text{Ni}_{0.3}\text{Zn}_{0.4}\text{Mn}_{0.3}\text{Fe}_{1.99}\text{O}_4$ ferrites.

earth has indeed replaced iron and the cation distribution obtained from Rietveld refinement is reasonable.

The vibrational bands around 3400 cm^{-1} and 1600 cm^{-1} in the Fourier Transform Infrared (FTIR) spectra (Fig. 3) show the presence of moisture. Some weak absorption bands between 800 cm^{-1} and 1600 cm^{-1} show the presence of less organics. Importantly, the formation of ferrite was confirmed by FTIR spectra, since there are two typical absorption bands (ν_1 and ν_2) of ferrite corresponding to A-site and B-site, as shown in Fig. 3. Their peak values are depicted in Table 1. The frequency of tetrahedral absorption band is higher than that of octahedral site because the tetrahedral bond length (A-O) is less than that of octahedral bond length (B-O) [20]. It is consistent with the fact that the tetrahedral ionic radii (r_A) are less than the

octahedral ionic radii (r_B). From Table 1, it can be seen that ν_1 is almost unchanged for all specimens. However, after rare earth doping, ν_2 has a decrease. And as the atomic number of rare earth increases, ν_2 shifts to high frequency region. The shift of absorption band also can be explained by the bond length. So, r_A is a constant, leading to unchanged ν_1 . At the same time, the increase of r_B results in a decrease of ν_2 with the increase of rare earth atomic number. These results demonstrated the correction of cation distribution again.

The hysteresis loops of $\text{RE}_{0.01}\text{Ni}_{0.3}\text{Zn}_{0.4}\text{Mn}_{0.3}\text{Fe}_{1.99}\text{O}_4$ ferrites measured at room temperature are shown in Fig. 4(a). It can be thought as exhibiting the typical soft ferromagnetic properties of ferrite with a coercivity of about 8 Oe. And the saturation

Fig. 2. Rietveld refinement of XRD patterns for $\text{RE}_{0.01}\text{Ni}_{0.3}\text{Zn}_{0.4}\text{Mn}_{0.3}\text{Fe}_{1.99}\text{O}_4$ ferrites.Fig. 3. FTIR spectra of $\text{RE}_{0.01}\text{Ni}_{0.3}\text{Zn}_{0.4}\text{Mn}_{0.3}\text{Fe}_{1.99}\text{O}_4$ ferrites.

magnetization (M_s) is shown in Table 2. It can be seen that the saturation magnetization of rare earth doped ferrite is slightly smaller than that of undoped ferrite. The same results were observed by

Table 1
absorption bands of all the samples.

RE	ν_1 (cm^{-1})	ν_2 (cm^{-1})
Fe	570	395
La	568	388
Nd	567	388
Sm	568	389
Gd	567	390
Dy	569	393
Yb	568	395

other researchers [21–23]. However, the saturation magnetization of different rare earth doped systems has no obvious regularity. It is also not related with particle size (Fig. 1) and bond length. As we all know, saturation magnetization is an intrinsic physical quantity, which mainly depends on the cation distribution. In order to explore the effect of cation distribution, based on the molecular formula obtained from refinement, the theoretical molecular magnetic moment of all samples is calculated (Fe^{3+} : $5\mu_B$, Mn^{2+} : $5\mu_B$, Ni^{2+} : $3\mu_B$, Zn^{2+} : $0\mu_B$, La^{3+} : $0\mu_B$, Nd^{3+} : $3.62\mu_B$, Sm^{3+} : $0.84\mu_B$, Gd^{3+} : $7.94\mu_B$, Dy^{3+} : $10.5\mu_B$ and Yb^{3+} : $4.5\mu_B$) to be about $6.4\mu_B$. It doesn't change for all samples, due to little doping. In addition, the experimental Bohr magnetic moment (n_B) can be calculated by the following formula.

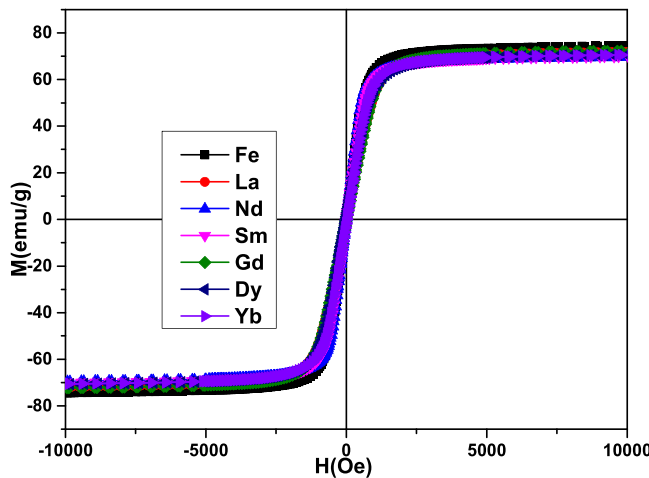
Fig. 4. The hysteresis loops of $\text{RE}_{0.01}\text{Ni}_{0.3}\text{Zn}_{0.4}\text{Mn}_{0.3}\text{Fe}_{1.99}\text{O}_4$ ferrites.

Table 2
magnetic parameters of $\text{RE}_{0.01}\text{Ni}_{0.3}\text{Zn}_{0.4}\text{Mn}_{0.3}\text{Fe}_{1.99}\text{O}_4$ ferrites.

	Fe	La	Nd	Sm	Gd	Dy	Yb
$M_s(\text{emu/g})$	74	72	70	70	72	71	71
$n_B (\mu_B)$	3.1	3.1	3.0	3.0	3.1	3.0	3.0

$$n_B = \frac{M_w \times M_s}{5585}$$

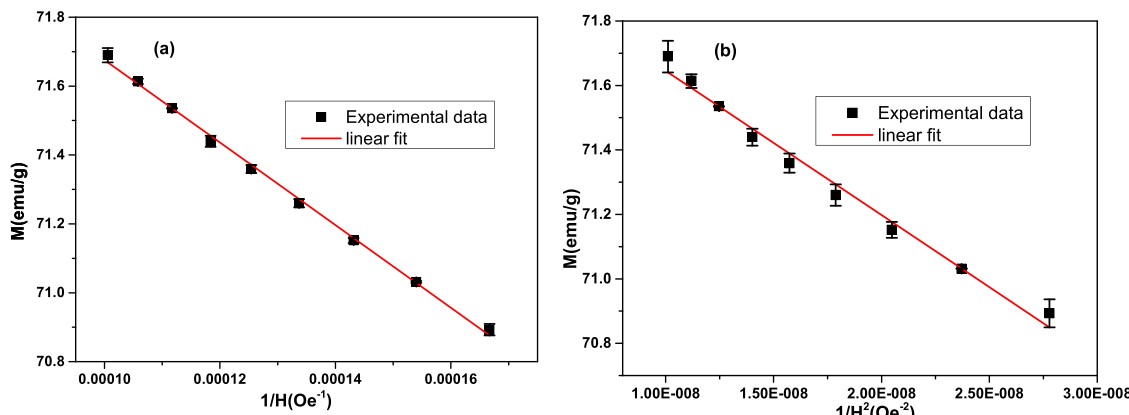
In which, M_w is relative molecular mass. The Bohr magnetic moment of $\text{RE}_{0.01}\text{Ni}_{0.3}\text{Zn}_{0.4}\text{Mn}_{0.3}\text{Fe}_{1.99}\text{O}_4$ ($\text{RE}=\text{Fe, La, Nd, Sm, Gd, Dy, Yb}$) shown in Table 2, is nearly constant and dose not depends on the doping of rare earth, which is consistent with the theoretical Bohr magnetic moment. The result demonstrates that the cation distribution can completely explain the magnetic change. It is similar with other reports[13,24].

In "Law of Approach to saturation" model [22],

$$M = M_s \left(1 - \frac{A}{H} - \frac{B}{H^2} \right) + \chi H$$

where, A/H term depends on inhomogeneities of samples, like gap, weak ferromagnetic or non-ferromagnetic phases, local deformation in crystal and so on, which make the magnetization in the crystal uneven, thus preventing it from reaching saturation. B/H^2 term depends on Magnetocrystalline anisotropy. χH is high-field paramagnetic term, which is considered in high-temperature analysis.

Two factors (inhomogeneity and magnetocrystalline anisotropy) are considered separately. Magnetization versus $1/H$ and $1/H^2$ plots

Fig. 5. magnetization versus $1/H$ (a) and $1/H^2$ (b) plots for Dy-NiZnMn ferrite. The data is linear fitted by using "Law of Approach to saturation".

for Dy-NiZnMn ferrite are linear fitted by using "Law of Approach to saturation", as shown in Fig. 5. The results show that magnetization is approximately linear with $1/H$, implying that inhomogeneities of samples can not be ignored. It is consistent with the porous microstructure (Fig. 1) and the view in reference 5.

Fig. 6(a-g) shows ZFC-FC magnetization curves measured in the temperature range from 10 K to 400 K with external field of 100 Oe. In the absence of an external field, the samples was cooled from room temperature to 10 K, and then ZFC curve was measured when the temperature increases to 400 K at 100 Oe. While FC curve was measured with the same external magnetic field during cooling the sample to 10 K. When the samples was cooled down to 10 K with zero filed, The magnetic moments of particles are frozen in their respective easy magnetization directions. Because the easy magnetization directions of particles in space are random, the total magnetic moment of the sample is very small. With the increases of the temperature, M_{ZFC} gradually build up due to thermal energy and the magnetic field of 100 Oe.

In addition, M_{FC} and M_{ZFC} curves do not coincide over the entire temperature range, and the measured M_{FC} value is significantly higher than M_{ZFC} value. The lower the temperature, the greater the difference between the two values, showing obvious thermo-magnetic irreversibility. From Fig. 6(a-g), M_{FC} and M_{ZFC} curves separation temperature(T_{irr} : the transition temperature from irreversibility to reversibility) for all samples is higher than 400 k. The split behavior of M_{FC} and M_{ZFC} curves is typical characteristics of some magnetic frustration system (superparamagnetism, spin glass, etc.). Most researchers [21,25] have observed this split phenomenon in ferrite nanoparticles, and T_{irr} is lower than room temperature. Syed Ismail Ahmada [26] reported that the blocking temperature (T_B) of Ce and Sm co-substituted nanaocrystalline cobalt ferrite is above 300 K, due to large particle size and small inter-particle spacing. Suman Sharma [13] reported that T_B is about 800 K in Rare-earth doped Ni-Co ferrites and increases with growing particle size.

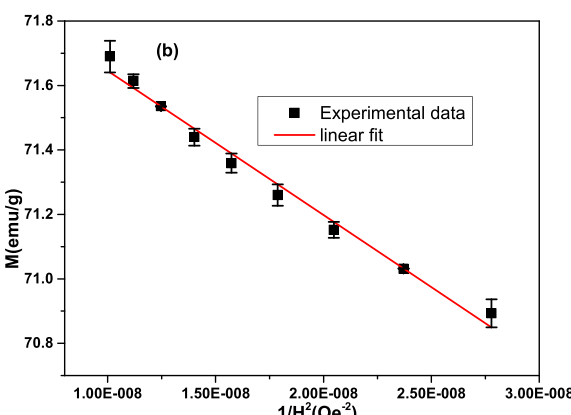
According to the Néel-Brown equation [25],

$$T_B = \frac{KV}{25k_B}$$

in which, K is the anisotropy constant, k_B is Boltzmann constant, and V is mean particle size (seen from Fig. 1) can results in high T_B and T_{irr} . Below T_B , the separation of M_{FC} and M_{ZFC} curves is due to freezing of disorder surface spin.

In fact, Mn ions will weaken the superexchange interaction between tetrahedral and octahedral ions [27,28], which will induce canting spin of the magnetic moment in the octahedral site [28]. Canting spin often leads to spin glass behavior.

At last, inhomogeneous distribution of magnetic ions will cause uneven interaction between magnetic moments, so the magnetic



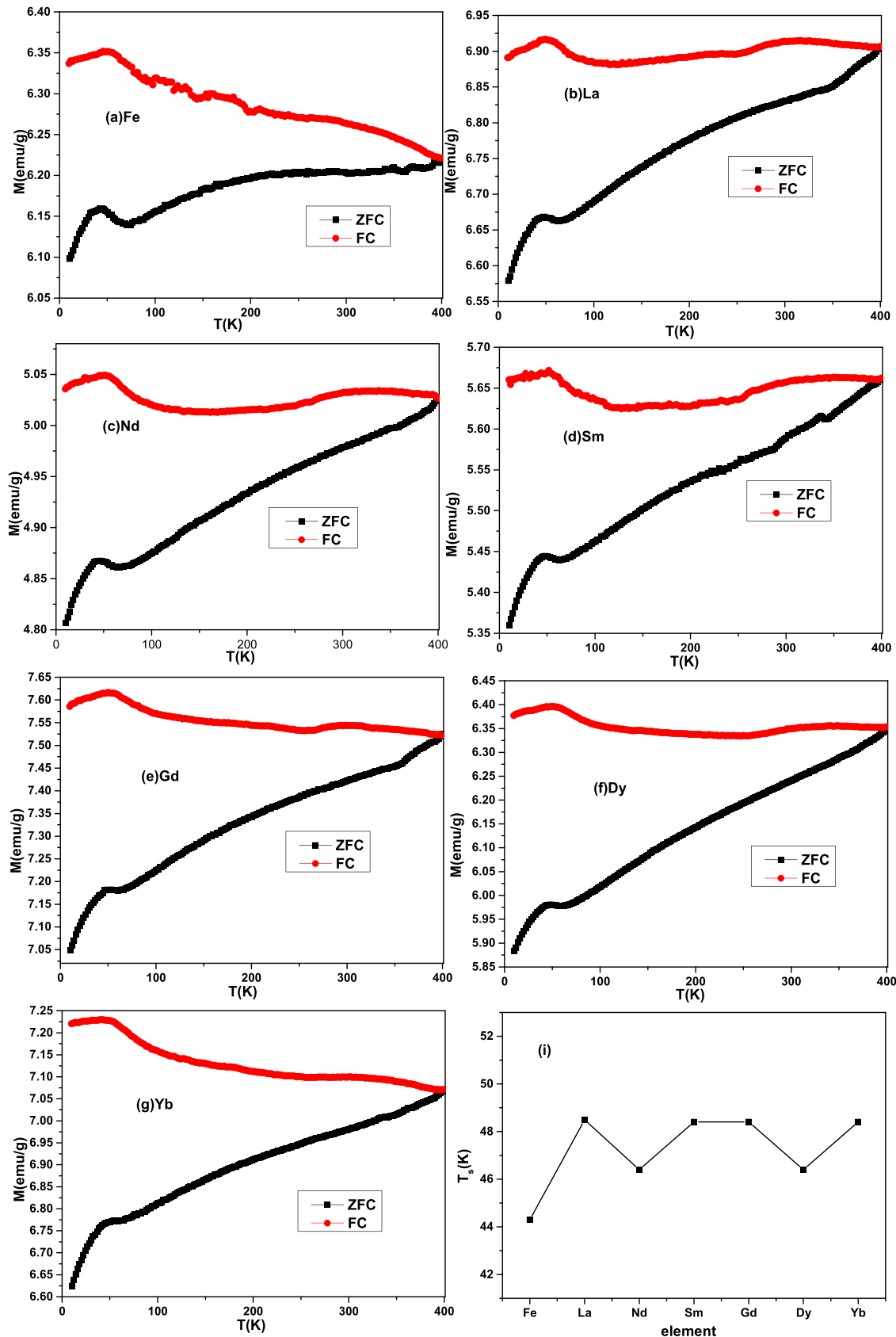


Fig. 6. ZFC-FC magnetization curves (a-g) and blocking temperature (i) for all samples.

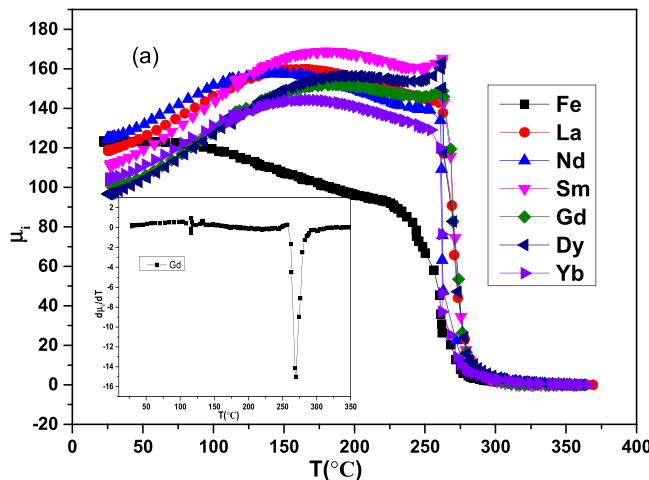


Fig. 7. the temperature dependence of the initial permeability of RE_{0.01}Ni_{0.3}Zn_{0.4}Mn_{0.3}Fe_{1.99}O₄ ferrites. The inset is $\frac{d\mu_i}{dT}$ plot of Gd-NiZnMn ferrite.

moment of the material is long-range disorder, and ZFC-FC curves are separated below 400 K.

ZFC-FC curves cannot distinguish these mechanisms. More work need to be done to understand low-temperature magnetism of RE-NiZnMn ferrite. Moreover, a peak at about 48 K in ZFC curves is observed in all samples. This means another magnetic phase transition. The phase transition temperature is almost a constant, independent of the doping of rare earth elements (Fig. 6(i)). So the magnetic phase transition maybe occur in ferrite nanoparticles (Fig. 1) or come from re-entrant spin glass behavior. There is not extra phase transition found in rare earth doped samples, showing the absence of rare earth-rich phase, which was also not found by XRD and IR analysis.

In order to further study the effect of rare earth on magnetic properties of NiZnMn ferrite, the temperature dependence of the initial permeability (μ_i) was measured, shown in Fig. 7. For the undoped NiZnMn ferrite, initial permeability firstly keeps constant from room temperature to 58 °C, then decreases with the increase of temperature, that is, the thermal coefficient of permeability is less than zero. For the rare earth-doped NiZnMn ferrite, initial permeability firstly increases until the temperature is up to about 160 °C, then decreases when the temperature continues to increase. The positive temperature coefficient below 160 °C indicates that the rare earth doped ferrite has good environmental adaptability[29].

According to magnetization theory,

$$\mu_i \propto \frac{M_s^2 d}{K}$$

where, K is anisotropy constant. Generally, magnetocrystalline anisotropy (K_1) of spinel NiZnMn ferrite is less than 0. Doping rare earth can distort the crystal structure of small domain around rare earth ions, and rearrangement of ions to low energy state may cause induced anisotropy $K_u > 0$. In addition, The addition of trivalent rare earth ions will increase Fe^{2+} ions with $K_1 > 0$. The Compensatory of these positive anisotropy leads to the appearance of peak in μ_i -T curve at 160 °C.

The Curie temperature (T_c) corresponds to the minimum slope in μ_i -T curves, which can be obtained by $\frac{d\mu_i}{dT}$ plot shown in the inset in Fig. 7. The initial permeability at room temperature and T_c of all samples are shown in Fig. 8. From Figs. 7 and 8, after doping rare earth, μ_i decreases due to the decrease of M_s . The initial permeability of La, Nd, Sm doped ferrite is greater than that of Gd, Dy and Yb doped ferrite. It is consistent with the mean particle size (Fig. 1). La,

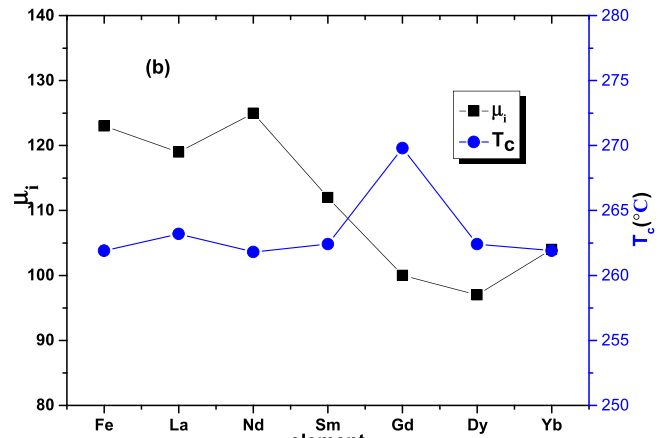


Fig. 8. μ_i and T_c of all samples.

Nd, Sm doped ferrite has a large particle size, and the blocking effect of grain boundary on domain wall displacement is small, so μ_i is large. Curie temperature is an intrinsic physical quantity, which depends on the interaction between tetrahedral magnetic ions and octahedral magnetic ions. Figs. 7 and 8 demonstrate that T_c of almost all samples is 262 °C, meaning that a small amount of rare earth elements did not change the interaction intensity. The result is different with the reports [30,31], in which the addition of rare earth in ferrite increases the permeability and Curie temperature of the material. Hichem Huili [8] observed the unchanged Curie temperature in RE-doped CoNiZn ferrite.

The complex permeability spectra are shown in Fig. 9(a). The real part of complex permeability (μ') for all samples is basically close to the initial permeability (Fig. 8). μ' of undoped samples keeps a constant below 4 MHz, however, μ' of rare earth doped samples keeps a constant below 6 MHz. Thus it can be seen that a small amount of rare earth ions can improve the frequency range of materials to use. It also can be confirmed by the fact that the cut-off frequency (f_r) of rare earth doped ferrite, which corresponds to the peak value of μ'' (image part of complex permeability), is higher than that of undoped ferrite, as shown in Fig. 9(b). And f_r of all samples is observed to be higher than 26.8 MHz. These materials are suitable for high frequency applications. According to Snoek theory, the decreases of μ_i will be accompanied by the increase of f_r . The cut-off frequency of heavy rare earth doped ferrites is higher than that of light rare earth doped ferrites.

Fig. 10(a) shows the dielectric constant (ϵ') plots of RE_{0.01}Ni_{0.3}Zn_{0.4}Mn_{0.3}Fe_{1.99}O₄ ferrites. The dielectric constant of Sm, Gd and Dy doped ferrite rapidly decreases with the increase of frequency (f) from 1 MHz to 160 MHz. Then, as the frequency continues to increase up to 1.8 GHz, the dielectric constant slowly decreases. This declining trend can be explained by polarization mechanism. At low frequency, more than one polarization (e.g. space charge polarization and electronic polarization etc) are present, so dielectric constant rapidly decreases. But, as applied frequency increases, space charge polarization will cease at some frequency, causing the slow decline of dielectric constant at high frequency. Above 1.8 GHz, two resonance peaks appear due to the matching of hopping frequency and the applied frequency, which was also observed in rare earth doped X-type hexagonal ferrites by Abdul Majed [12]. For other samples, this relaxation process at low frequency is different. The dielectric constant keep unchanged as the applied frequency is low. From Fig. 10(a), it can be seen that the dielectric constant increases after doping rare earth. Xiao-Hui Wu [32] reported the similar result in Y-doped NiZnCo ferrites, because the hopping of electron increases with the decrease of porosity and the increase of Fe^{2+} due to the formation of second phase. Charalampos Stergiou

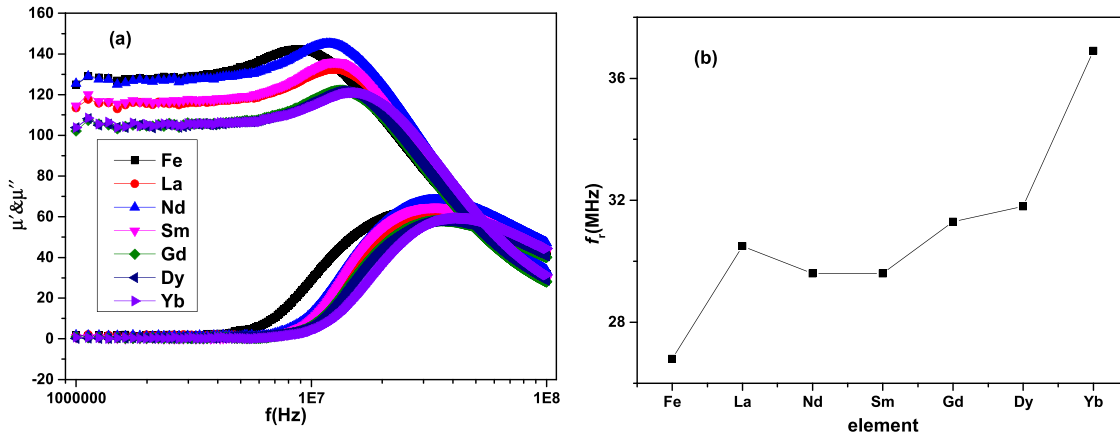


Fig. 9. the complex permeability spectra (a) and the cut-off frequency (b) of all samples.

[33] thought doping rare earth can lead to cation vacancies, thus forming electric dipole which can enhance the dielectric constant.

ϵ'' is symbol of dielectric loss, shown in Fig. 10(b). ϵ'' of rare earth doped ferrite is larger than that of undoped ferrite, showing better electromagnetic wave absorption properties. As frequency increases in the range of 1 MHz to 2 GHz, dielectric loss increases at first, and then decreases. This result dose not follow Maxwell Wagner's and Koop's theories of ferrite's double layered structure, whose ϵ'' firstly decreases and then keep constant with the increase of frequency [34]. This trend shows that the relaxation process is related with Debye dipolar model.

$$\epsilon' = \epsilon_\infty + \frac{\epsilon_s - \epsilon_\infty}{1 + (2\pi f)^2 \tau^2}$$

$$\epsilon'' = \frac{(\epsilon_s - \epsilon_\infty)2\pi f\tau}{1 + (2\pi f)^2 \tau^2}$$

where, ϵ_∞ is dielectric constant at infinite frequency, ϵ_s is the static dielectric constant, and τ is relaxation time.

$$[\epsilon' - \frac{1}{2}(\epsilon_s + \epsilon_\infty)]^2 + (\epsilon'')^2 = \frac{1}{4}(\epsilon_s + \epsilon_\infty)^2$$

From Fig. 10(c), the circle was observed in low ϵ' region, (i.e. high frequency section) for all samples. This distorted semi-circle suggests the existence of other mechanism[35], like as resonance. In high ϵ' range, the $\epsilon''-\epsilon'$ curve of La, Nd, Yb doped and pure NiZnMn ferrite has a semicircle, which represents one relax mechanism. However, the $\epsilon''-\epsilon'$ curves of Sm, Gd and Dy doped ferrite (in

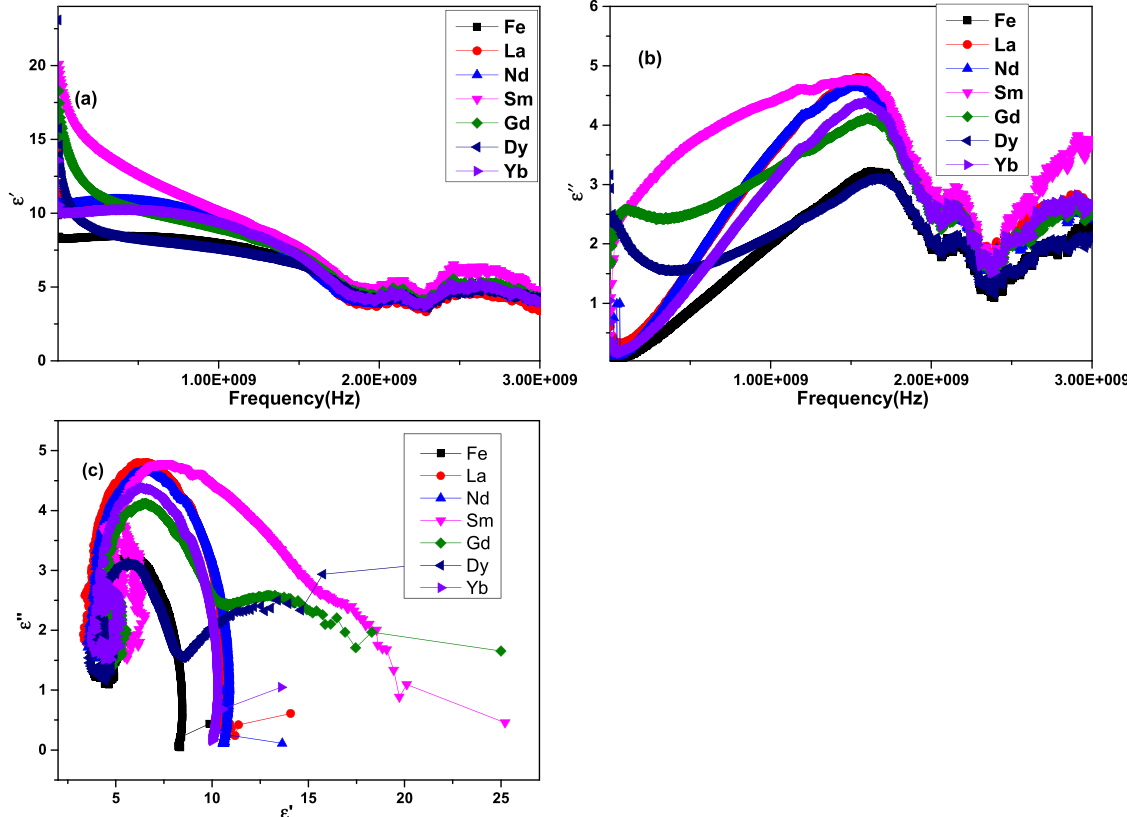


Fig. 10. Dielectric constant ϵ' (a) and dielectric loss factor ϵ'' (b) versus frequency plots, Relationship between real and imaginary part of permittivity (c).

Fig. 10(c)) have two semi-circles, demonstrating that there are two dielectric relaxation processes.

4. Conclusions

In summary, rare-earth doped NiZnMn spinel ferrite with the strictly controlled main composition were prepared in this work. Some same impacts of all rare earth on structure and electromagnetic properties of NiZnMn ferrite were observed. After rare earth doping, the average particle size (d), the saturation magnetization (M_s) and initial permeability (μ_i) decrease, while, the thermal coefficient, dielectric constant and loss increases due to induced Fe^{2+} ions. Almost all samples have the same Curie temperature (262 °C). ZFC-FC curves demonstrate the existence of spin glass state or superparamagnetism at high temperature.

The change of structure is basically consistent with the radii of rare earth ions. However, the magnetic properties do not show a dependence on rare earth. Particle size plays a major role on intial permeability. In addition, dielectric study displays more relaxation processes occurring in the Sm, Gd and Dy doped ferrites.

The cut-off frequency of all samples is higher than 26.8 MHz, showing that these materials can be applied in high frequency devices. And rare earth doping can improve the cut-off frequency.

CRediT authorship contribution statement

Xueyun Zhou: Methodology, Writing - original draft. **Jun Wang:** experiment, measurement of data. **Dongsheng Yao:** data analysis and check the figures.

Data Availability

The datasets generated during and/or analysed during the current study are available from the corresponding author on reasonable request.

Declaration of Competing Interest

The authors declare the following financial interests/personal relationships which may be considered as potential competing interests: Xueyun Zhou reports financial support was provided by National Natural Science Foundation of China (51962016). Xueyun Zhou reports financial support was provided by Fundamental Research Funds for the Central Universities of Civil Aviation University of China (3122021123).

Acknowledgements

This work was supported by National Natural Science Foundation of China (51962016); Fundamental Research Funds for the Central Universities of Civil Aviation University of China (3122021123).

References

- [1] preeti Thakur, Deepika Chahar, Shilpa Taneja, Nikhil Bhalla, Atul Thakur, A review on MnZn ferrites: synthesis, characterization and applications, *Ceramics Int.* 46 (2020) 1740.
- [2] JinAh Hwang, Moonhee Choi, Hyo-soon Shin, Byeong-Kwon Ju, MyoungPyo Chun, Structural and magnetic properties of NiZn ferrite nanoparticles synthesized by a thermal decomposition method, *Appl. Sci.* 10 (2020) 6279.
- [3] S. Mallesh, V. Srinivas, A comprehensive study on thermal stability and magnetic properties of MnZn-ferrite nanoparticles, *J. Magn. Magn. Mater.* 475 (2019) 290.
- [4] Zhanyuan Xu, Jinglian Fan, Tao Liu, Yong Han, Hongbo Zhang, Calcination induced phase transformation in MnZn ferrite powders, *J. Alloy. Compd.* 814 (2020) 152307.
- [5] G. Fraker, O. Isnard, H. Chazal, G. Delette, Effect of cobalt addition on the mageto-crystalline anisotropy parameter of sintered NiZn ferrites evaluated from magnetization curves, *J. Magn. Magn. Mater.* 473 (2019) 92.
- [6] Xueyun Zhou, Jun Wang, Liling Zhou, Dongsheng Yao, The improved saturation magnetization and initial permeability in Mn-NiZn ferrites after cooling in vacuum, *Appl. Phys. A* 128 (2022) 306.
- [7] Zhiqing Liu, Zhijian Peng, Changchun Lv, Xiuli Fu, Doping effect of Sm^{3+} on magnetic and dielectric properties of Ni-Zn ferrites, *Ceram. Int.* 43 (2017) 1449.
- [8] Hichem Huili, Ali Mater, Bilel Grindi, Guillaume Viau, Abdessalem Kouki, Lotfi Ben Tahar, Influence of the RE_2O_3 ($RE = Y, Gd$) and CaO nanoadditives on the electromagnetic properties of nanocrystalline $Co_{0.2}Ni_{0.3}Zn_{0.5}Fe_2O_4$, *Arab. J. Chem.* 12 (2019) 489.
- [9] Rakesh Kumar Singh, Jyoti Shah, R.K. Kotnala, Magnetic and dielectric properties of rare earth substituted $Ni_{0.5}Zn_{0.5}Fe_{1.95}R_{0.05}O_4$ ($R = Pr, Sm$ and La) ferrite nanoparticles, *Mater. Sci. Eng. B* 210 (2016) 64.
- [10] Zhou Xueyun, Zhou Yuxiu, Zhou Liling, Wei Jianning, Wu Junqing, Dongsheng Yao, "Effect of Gd and La doping on the structure, optical and magnetic properties of NiZnCo ferrites", *Ceram. Int.* 45 (2019) 6236.
- [11] Yanchun Zhang, Aimin Sun, Zhai Xuinan, Effect of rare-earth (Sm, Ce, and La) ions doping on the lattice structure and magnetic properties of Zn-Ba-Co ferrites by sol-gel auto-combustion method, *J. Mater. Sci: Mater. Electron.* 32 (2021) 16505.
- [12] Abdul Majeed, Muhammad Azhar Khan, Faseeh ur Raheem, Iftikhar Ahmad, Majid Niaz Akhtar, Muhammad Farooq Warsi, Morphological, Raman, electrical and dielectric properties of rare earth doped X-type hexagonal ferrites, *Phys. B* 503 (2016) 38.
- [13] Suman Sharma, Mukesh Kumar Verma, Narayan Dutt Sharma, Nisha Choudhary, Sumit Singh, Devinder Singh, Rare-earth doped Ni-Co ferrites synthesized by Pechini method: Cation distribution and high temperature magnetic studies, *Ceram. Int.* 47 (2021) 17510.
- [14] Xueyun Zhou, Jun Wang, Liling Zhou, Dongsheng Yao, Structure, magnetic and microwave absorption properties of NiZnMn ferrite ceramics, *J. Magn. Magn. Mater.* 534 (2021) 168043.
- [15] D. Li, Y. Sun, Y. Xu, H. Ge, Q. Wu, C. Yan, Effects of Dy^{3+} substitution on the structural and magnetic properties of $Ni_{0.5}Zn_{0.5}Fe_2O_4$ nanoparticles prepared by a sol-gel self-combustion method, *Ceram. Int.* 41 (2015) 4581.
- [16] Lalita Chauhan, Nidhi Singh, Ajay Dhar, Harsh Kumar, Sudhanshu Kumara, K. Sreenivas, Structural and electrical properties of Dy^{3+} substituted $NiFe_2O_4$ ceramics prepared from powders derived by combustion method, *Ceram. Int.* 43 (2017) 8378.
- [17] Fumie Hirosawa, Tomohiro Iwasaki, A comparative study of the magnetic induction heating properties of rare earth (RE = Y, La, Ce, Pr, Nd, Gd and Yb)-substituted magnesium-zinc ferrites, *Solid State Sci.* 118 (2021) 106655.
- [18] Lovely George, C. Viji, M. Maheen, E.M. Mohammed, Enhanced magnetic properties at low temperature of Mn substituted Ni-Zn mixed ferrite doped with Gd ions for magnetoresistive applications, *Mater. Res. Bull.* 126 (2020) 110833.
- [19] B. Parvatheswara Rao, B. Dhanalakshmi, S. Ramesh, P.S.V. Subba Rao, Cation distribution of Ni-Zn-Mn ferrite nanoparticles, *J. Magn. Magn. Mater.* 456 (2018) 444.
- [20] G.M. Shweta, L.R. Naik, R.B. Pujar, S.N. Mathad, Influence of magnesium doping on structural and elastic parameters of Nickel Zinc nanoferrites, *Mater. Chem. Phys.* 257 (2021) 123825.
- [21] M.A. Almessierea, S. Güner, Y. Slimani, A. Baykal, E. Sagar, A. Shirasath, R. Demir Korkmaz, A. Badar, Manikandan, Investigation on the structural, optical, and magnetic features of Dy^{3+} and Y^{3+} co-doped $Mn_{0.5}Zn_{0.5}Fe_2O_4$ spinel ferrite nanoparticles, *J. Mol. Struct.* 1248 (2022) 131412.
- [22] M. Maria Lumina Sonia, S. Anand, V. Maria Vinisel, M. Asisi Janifer, S. Pauline, A. Manikandan, Effect of lattice strain on structure, morphology and magneto-dielectric properties of spinel $NiGd_xFe_{2-x}O_4$ ferrite nano-crystallites synthesized by sol-gel route, *J. Magn. Magn. Mater.* 466 (2018) 238.
- [23] K.V. Zire, S.S. Bandgar, G.S. Shahane, Effect of Dy-substitution on structural and magnetic properties of Mn-Zn ferrite nanoparticles, *J. Rare Earths* 36 (2018) 86.
- [24] M.H. Abdellatif, G.M. El-Komy, A.A. Azab, Magnetic characterization of rare earth doped spinel ferrite, *J. Magn. Magn. Mater.* 442 (2017) 445.
- [25] Mrityunjay Prasad Ghosh, Samrat Mukherjee, Size variation in nanocrystalline $Zn_{0.2}Ni_{0.8}Gd_{0.05}Fe_{1.95}O_4$ ferrites: Exchange bias effect and its correlation with disordered surface spins, *Mater. Res. Bull.* 125 (2020) 110785.
- [26] Syed Ismail Ahmada, Abdul Rauf, Tasneem Mohammed, Amal Bahfi, D. Ravi Kumar, Madireddy Buchi Suresh, Dielectric, impedance, AC conductivity and low-temperature magnetic studies of Ce and Sm co-substituted nanocrystalline cobalt ferrite, *J. Magn. Magn. Mater.* 492 (2019) 165666.
- [27] U.B. Gawas, V.M.S. Verenkar, V.T. Vader, Anil Jain, Sher Singh Meena, Effects of sintering temperature on microstructure, initial permeability and electric behaviour of Ni-Mn-Zn ferrites, *Mater. Chem. Phys.* 275 (2022) 125250.
- [28] Sagar E. Shirasath, B.G. Toksha, R.H. Kadam, S.M. Patange, D.R. Mane, Ganesh S. Jangam, Ali Ghasemi, Doping effect of Mn^{2+} on the magnetic behavior in Ni-Zn ferrite nanoparticles prepared by sol-gel auto-combustion, *J. Phys. Chem. Solids* 71 (2010) 1669.
- [29] Kaiqi Jiang, Kangkang Li, Changhong Peng, Yun Zhu, Effect of multi-additives on the microstructure and magnetic properties of high permeability Mn-Zn ferrite, *J. Alloy. Compd.* 541 (2012) 472.
- [30] Le-Zhong Li, Xiao-Xi Zhong, Rui Wang, Xiao-Qiang Tu, Lei He, Feng-Hua Wang, Effects of Ce substitution on the structural and electromagnetic properties of NiZn ferrite, *J. Magn. Magn. Mater.* 475 (2019) 1.
- [31] M.M. Eltabey, W.R. Agami, H.T. Mohsen, Improvement of the magnetic properties for Mn-Ni-Zn ferrites by rare earth Nd^{3+} ion substitution, *J. Adv. Res.* 5 (2014) 601.

- [32] Xiao-Hui Wu, Le-Zhong Li, Bo Wu, Xiao-Xi Zhong, Rui Wang, Xiao-Qiang Tu, Lei He, Chen-Yu Zou, Bo-Ren Hou, Structure and enhanced electromagnetic properties of Y^{3+} substituted microwave sintered NiZnCo ferrites, Ceram. Int. 47 (2021) 3720.
- [33] Charalampos Stergiou, Magnetic, dielectric and microwave absorption properties of rare earth doped Ni-Co and Ni-Co-Zn spinel ferrites, J. Magn. Magn. Mater. 426 (2017) 629.
- [34] Asima Anwar, Muhammad Asif Yousuf, Sonia Zulfiqar, Philips O. Agboola, Imran Shakir, Najeeb Faud Al-Khalli, Muhammad Farooq Warsi, The impact of highly paramagnetic Gd^{3+} cations on structural, spectral, magnetic and dielectric properties of spinel nickel ferrite nanoparticles, J. Saudi Chem. Soc. 25 (2021) 101306.
- [35] Tao Ma, Yu Cui, Yulin Sha, Li Liu, Jianwen Ge, Fandi Meng, Fuhui Wang, Facile synthesis of hierarchically porous rGO/MnZn ferrite composites for enhanced microwave absorption performance, Synth. Met. 265 (2020) 116407.